

Kaluza-Klein Dark Matter and Galactic Antiprotons

Aurelien Barrau*

*Laboratory for Subatomic Physics and Cosmology
CNRS-IN2P3 and Université Joseph Fourier
53, avenue des Martyrs, 38026 Grenoble cedex, France*

Pierre Salati†

*Laboratoire d'Annecy-le-Vieux de Physique Théorique
CNRS-SPM and Université de Savoie
9, Chemin de Bellevue,
B.P.110 74941 Annecy-le-Vieux, France*

Géraldine Servant‡

*Service de Physique Théorique
CEA Saclay
91191 Gif-sur-Yvette Cédex, France*

Fiorenza Donato

*Dipartimento di Fisica Teorica and INFN, Torino
via Giuria 1, 10125 Torino, Italy*

Julien Grain

*Laboratory for Subatomic Physics and Cosmology
CNRS-IN2P3 and Université Joseph Fourier
53, avenue des Martyrs, 38026 Grenoble cedex, France*

David Maurin

*Service d'Astrophysique DSM/SAP
Orme des Merisiers, CEA/Saclay
91191 Gif-sur-Yvette Cedex, France*

Richard Taillet

*Université de Savoie, 73000 Chambéry, France
LPNHE, Jussieu, CNRS-IN2P3, Paris, France
(Dated: June 15, 2005)*

Extra dimensions offer new ways to address long-standing problems in beyond the standard model particle physics. In some classes of extra-dimensional models, the lightest Kaluza-Klein particle is a viable dark matter candidate. In this work, we study indirect detection of Kaluza-Klein dark matter via its annihilation into antiprotons. We use a sophisticated galactic cosmic ray diffusion model whose parameters are fully constrained by an extensive set of experimental data. We discuss how fluxes of cosmic antiprotons can be used to exclude low Kaluza-Klein masses.

PACS numbers: 95.35.+d (dark matter), 04.50.+h (Kaluza-Klein theory), 98.70.Sa (Cosmic-rays)

*Electronic address: Aurelien.Barrau@cern.ch

†Electronic address: Salati@lapp.in2p3.fr

‡Electronic address: servant@spht.saclay.cea.fr

I. INTRODUCTION

Non-baryonic dark matter has been shown to be the dominant matter component of our Universe by several independent measurements – see [1] for a review. The recently published WMAP results [2], combined with ACBAR, CBI and 2dFGRS, lead to precise estimates of the baryonic, matter and total densities : $\Omega_b h^2 = 0.0224 \pm 0.0009$, $\Omega_m h^2 = 0.135 \pm 0.009$ and $\Omega_{tot} = 1.02 \pm 0.02$. Weakly Interacting Massive Particles (WIMPs) are the favourite candidates to account for the Cold (non-baryonic) Dark Matter (CDM) as the required relic density can be naturally generated. Theoretically well-founded, neutralinos are certainly the most extensively studied example. On the other hand, in spite of the very important efforts devoted to direct and indirect searches in this direction, supersymmetric particles have not yet been discovered and alternative candidates should be considered. Among them, Kaluza-Klein (KK) particles are promising. So far, they arise as stable viable WIMPs in two frameworks : In Universal Extra Dimensions (UED) [3] and in some warped geometries à la Randall-Sundrum [4].

In the case of UED, all standard model fields propagate in one or more flat compact extra dimensions – unlike models with Large Extra Dimensions à la ADD [5]. As a result, the combination of a translation by πR with a flip of sign of all odd states in the KK Fourier decomposition of the bulk fields – named KK-parity – is conserved. This implies that the lightest first level KK particle (LKP) cannot decay into standard model modes and is stable. Such a Kaluza-Klein particle is likely to be associated with the first KK excitation of the photon, more precisely the first excitation of the hypercharge gauge boson [6], and is referred to as $B^{(1)}$. Depending on the number of dimensions and on the mass difference between the LKP and the NLKP – next to LKP – the $B^{(1)}$ mass is expected to lie in the range 300 – 1000 GeV if it is to account for dark matter [7] – for a recent analysis see [8]. Although not very narrow, this range is much smaller than in the neutralino case and this approach has much less free parameters. Furthermore, this range is fully compatible with experimental constraints which lead – in the $D = 5$ case – from precision electroweak measurements to compactification radii satisfying $R^{-1} \gtrsim 300$ GeV. Direct detection of the $B^{(1)}$ LKP has been studied in germanium, sodium iodine and xenon detectors [9, 10]. Indirect detection through gamma-rays [10, 11, 12, 13, 14], neutrinos and synchrotron flux [11], or through positrons [10, 15] has also been considered. The neutrino spectrum from LKP annihilation in the Sun was investigated in [16]. Constraints on UED models from radion cosmology have also been studied [17].

The second class of Kaluza-Klein WIMPs arises in higher dimensional warped Grand Unified Theories [18, 19]. In these models, a stable KK fermion can arise as a consequence of imposing proton stability in a way very reminiscent to R-parity stabilizing the lightest supersymmetric particle in supersymmetric models. The symmetry is called Z_3 and the Lightest Z_3 Particle (LZP) is stable since it cannot decay into standard model particles. It is actually associated with a KK Dirac right-handed neutrino with a mass in the 1 GeV to 1 TeV range. This RH neutrino has gauge interactions in particular with additional KK Z' gauge bosons. Nevertheless, its interactions with ordinary matter are feeble because they involve heavy gauge bosons with a mass $\gtrsim 3$ TeV. This opens the possibility of a weakly heavy gauge bosons with a mass $M_{KK} \gtrsim 3$ TeV. This opens the possibility of a weakly interacting Dirac RH neutrino. Indirect detection of “warped dark matter” in neutrino telescopes, gamma ray telescopes and cosmic positron experiments was investigated in [20]. In principle, the LZP is not necessarily the lightest KK particle. There might be lighter KK modes but which are unstable because they are not charged under Z_3 . In practise though, and in the models of [18, 19], the RH neutrino LZP turns out to be the lightest KK particle due to various phenomenological constraints. Thus, in the following, we will use the generic appellation “LKP” for both UED and warped types of KK dark matter.

In the present paper, we study the cosmic antiprotons that should be emitted as a result of LKP annihilations in the halo of the Milky Way. Those cosmic rays are of particular interest as the \bar{p}/p ratio is both small – smaller than 10^{-4} whatever the energy – and well-known [21]. The antiproton flux has been mostly measured by stratospheric balloon borne detectors – IMAX [22], MASS [23], CAPRICE [24, 25] and BESS [26, 27, 28] – flying at the top of the atmosphere. The interactions of high energy particles impinging on the latter generate a background to be removed in order to measure a signal that is compatible – given the uncertainties – with a pure secondary production arising from the spallations of cosmic ray nuclei on the interstellar gas of the Milky Way disk. The antiproton flux will be measured with unprecedented accuracy by the forthcoming space experiment AMS [29] that has already flown on the space shuttle [30]. Small deviations from a pure secondary energy spectrum – expected in our case if LKP particles annihilate in the galactic halo – are potentially detectable by AMS. In section II, the source term is computed by convolving the LKP number density and cross sections with the relevant fragmentation functions. Section III is devoted to the propagation scheme and the astrophysical parameters. Finally, the primary antiproton flux resulting from LKP annihilations is compared in section IV with the secondary background and some perspectives are drawn. We will show that antiprotons can at least constrain the lowest values of LKP masses.

II. SOURCE TERM

The production rate $q_{\bar{p}}^{\text{LKP}}$ of antiprotons is obtained from the convolution over the various annihilation channels f of the appropriate annihilation cross section $\langle \sigma v \rangle_f$ with the fragmentation function $(dN_{\bar{p}}/dT_{\bar{p}})_f$. It can be written as :

$$q_{\bar{p}}^{\text{LKP}}(r, T_{\bar{p}}) = \frac{1}{2} \sum_{\text{channel } f} \langle \sigma v \rangle_f \left(\frac{dN_{\bar{p}}}{dT_{\bar{p}}} \right)_f \left\{ n_{\text{LKP}}(r) \equiv \frac{\rho_{\text{LKP}}(r)}{M_{\text{LKP}}} \right\}^2. \quad (1)$$

The LKP particles in the initial state are identical hence the overall factor of 1/2. The distance between the production point and the galactic center is denoted by r while $n_{\text{LKP}}(r)$ and $\rho_{\text{LKP}}(r)$ respectively stand for the LKP number and mass densities. Antiprotons are produced with a kinetic energy $T_{\bar{p}}$ that ranges from 0 up to the LKP mass M_{LKP} . The previous relation features the four key ingredients that participate into the Kaluza-Klein antiproton source term $q_{\bar{p}}^{\text{LKP}}$.

To commence, for UED dark matter, the LKP annihilation cross section into fermions is given in the non-relativistic expansion limit by [7] :

$$\sigma |\vec{v}_1 - \vec{v}_2| \left\{ B^{(1)} B^{(1)} \rightarrow f \bar{f} \right\} = \frac{8\pi}{9} N_c (Y_L^4 + Y_R^4) \frac{\alpha_1^2}{M_{\text{LKP}}^2} (1 - v^2), \quad (2)$$

where N_c , Y_L and Y_R are respectively the number of colors and the left and right hypercharges of the resulting fermion f whereas $2\vec{v} = \vec{v}_1 - \vec{v}_2$. Velocities within the Milky Way are typically non-relativistic so that the factor $1 - v^2$ can safely be approximated by 1. Notice that in contrast with neutralino dark matter, the annihilation into fermions is not helicity-suppressed. For warped dark matter, there is no simple analytical formula – in particular, couplings depend in a non-trivial way on the LKP mass – but we can summarize the situation as follows. For LKPs lighter than approximately 100 GeV, LKP annihilations proceed dominantly via s-channel Z -exchange. For larger masses, annihilation into top quarks via the t-channel exchange of the GUT KK gauge boson X_s or into $t\bar{t}$, $b\bar{b}$, W^+W^- and Zh via the s-channel KK Z' exchange dominates. We refer the reader to the appendices of [19] for details. In the rest of the paper, we have taken a Kaluza-Klein gauge boson mass of $M_{\text{KK}} = 3$ TeV and varied the LKP mass from 30 to 70 GeV. Median values for the annihilation cross section have been assumed here. They correspond to the couplings $g_{10} = (g' + g_s)/2 = 0.785$ and $c_{\nu'_L} = 0.4$.

The second ingredient is the computation of the number of antiprotons with kinetic energy between $T_{\bar{p}}$ and $T_{\bar{p}} + dT_{\bar{p}}$ formed within a jet induced by a $q\bar{q}$ pair of energy M_{LKP} . This was evaluated with the high-energy physics frequently-used Monte-Carlo event generator PYTHIA [31], based on the so-called string fragmentation model.

The square of the LKP number density n_{LKP} enters into the annihilation rate (1) and scales as M_{LKP}^{-2} . In UED models, the LKP requires a mass in the range between 700 and 900 GeV in order to generate the observed thermal relic density, unless other KK modes participate in the freeze-out process [7]. If this is the case, somewhat smaller masses are possible. A recent analysis, taking into account the effects of second level KK modes, indicates that the upper edge of this mass range is favored [8]. In any case, we should keep in mind that the precise prediction of the LKP relic density depends on the particular KK mass spectrum which is used and is somewhat model-dependent. We will therefore consider masses in the lower range ~ 300 GeV which is the most favorable case as far as the antiproton signal is concerned. As for the warped LKP, it can thermally generate the observed quantity of dark matter in two mass ranges : near the Z -resonance with $M_{\text{LKP}} \approx 20$ to 80 GeV and for considerably heavier masses – $M_{\text{LKP}} \gtrsim$ several hundred GeV – [18, 19]. Again, we will restrict ourselves to the more easily accessible lowest masses.

The distribution of dark matter inside galaxies is still an open and very debated issue. From one side, results from cosmological N-body simulations in Λ -CDM models [32, 33, 34] indicate a universal and coreless dark matter density profile. At small radii, the latter diverges with the distance r from the galactic center as $r^{-\gamma}$ with $\gamma \sim 1$ to 1.5. This implies a strongly peaked dark matter density at galactic centers. Very recent results obtained from simulations of halo formation [35, 36] strongly disfavour a singularity as steep as 1.5 and seem to point toward slopes logarithmically dependent on the distance from the galactic center and no steeper than ~ 1.2 . It should indeed be noticed that these cusps are predicted in regions which are usually smaller than the typical resolution size of the simulations. On the other side, several analysis of rotational curves observed for galaxies of different morphological types [37, 38, 39, 40, 41, 42] put serious doubts on the existence of dark matter cusps in the central regions of the considered objects. Instead of a central singularity, these studies rather suggest a cored dark matter distribution, flattened toward the central regions. In the present analysis, we will consider the generic dark matter distribution

$$\rho_{\text{CDM}}(r) = \rho_{\text{CDM} \odot} \left\{ \frac{r_{\odot}}{r} \right\}^{\gamma} \left\{ \frac{1 + (r_{\odot}/a)^{\alpha}}{1 + (r/a)^{\alpha}} \right\}^{(\beta-\gamma)/\alpha}, \quad (3)$$

where $r_{\odot} = 8$ kpc is the distance of the Solar System from the galactic center. The local – Solar System – CDM density has been set equal to $\rho_{\text{CDM } \odot} = 0.3 \text{ GeV cm}^{-3}$. In the case of the pseudo-isothermal profile, the typical length scale a is the radius of the central core. The profile indices α , β and γ for the dark matter distributions which we have considered here are indicated in Tab. I. As already underlined in [44, 45] – and as it will be clear also from the

Halo model	α	β	γ	a [kpc]
Cored isothermal [43]	2	2	0	4
Navarro, Frenk & White [32]	1	3	1	25
Moore [34]	1.5	3	1.3	30

TABLE I: Dark matter distribution profiles in the Milky Way.

results presented in the following of the present paper – the diffusion of primary CDM generated antiprotons is only very mildly dependent on the chosen dark matter distribution function.

III. GALACTIC PROPAGATION: CONTROL OF UNCERTAINTIES

Propagation in the Galaxy, while studied for a long time is not a simple matter. A realistic description should take into account the coupling between gas, magnetic field and cosmic rays (CRs). This is far from being reached – at least at the Galactic scale. Our lack of knowledge about the structure of magnetic turbulences and their spatial distribution – probably related to the regions of star formation – hampers any clear and unambiguous description of the transport of CRs. So far, one major approximation assumed in all – but a very few number – of papers is that diffusion in the Galaxy does not depend on the galactic position. Even with this simplification, transport of CRs is not straightforward. It involves the now classical following ingredients : diffusion – random walk on magnetic inhomogeneities – and convection – directed outward the galactic disk – which compete for the spatial transport, especially at low energy. Regarding the energetic balance, energy losses – Coulomb, ionization and adiabatic – replenish the low energy tail whereas momentum diffusion – reacceleration – produces, on average, a gain in energy in the GeV/nucleon region. Finally, spallations may destroy CRs, preferentially at low energies.

Whatever the model retained for propagating antiprotons, it is very important to understand the origin of uncertainties in the propagated spectra. At a given energy E , spatial transport is sensitive to the following parameters – see Fig. 2 in [46] : the diffusion coefficient normalization and slope in $K(E) = \beta K_0 \mathcal{R}^{-\delta}$ where the rigidity $\mathcal{R} = p/Z$, the halo height L , the wind velocity V_c perpendicular to the disk – chosen to be constant in our model – and the Alfvénic speed V_a of the scatterers – the uncertainty due to this latter parameter is less significant compared to the previous processes. Only special combinations of these parameters can account for the measured B/C ratio. The abundance of boron relative to carbon – two typical elements which are respectively from secondary and primary origin – is a very good tracer of the history of CRs propagation. In a previous study, a degeneracy between these combinations was found [47], leading to a wide uncertainty in the underlying parameters of the model, although they gave the same B/C ratio. In a second study, the same combinations were used to compute the secondary antiproton signal in the same model [21]. The induced uncertainty for this secondary flux in the region of interest – a few hundreds of MeV – was found to be small – about 10%. This was expected, as all these species follow the same propagation paths, being emitted and detected in the disk.

The situation is quite different for primary exotic species, as most diffusion paths start in the diffusive halo [45, 48]. The previous degeneracy is broken. The induced uncertainties on primary antiprotons are studied in details in [44] and are found to be as large as a factor ~ 100 for supersymmetric particles. We briefly recall here, on a physical basis, the dependance of the uncertainty on each parameter, as it also applies to the present study. First, the halo height L determines i) the total number of sources inside the diffusive region and ii) the effective radial range of diffusion, i.e. the distance that a CR can travel from a source before escaping from the Galaxy. Cosmic rays coming from farther than L have an exponentially low probability to be detected on Earth. Notice that this second point explains why the evaluated fluxes are not very sensitive to the shape of the dark matter halo in the galactic center region – see below in section IV and in [44]. Second, the galactic wind wipes the particles away from the disk. It is well known that the effect of V_c is similar to that of L when sources are located in the disk – see [49] and $L^* \sim K(E)/L$ – but this is not true for sources in the halo. The two effects i) and ii) actually turn out to be of greater magnitude for L^* than for L .

It should be kept in mind that the parameters L , V_c and K_0 are correlated. In the subset of parameters giving the observed B/C ratio, low values of K_0 generally correspond to low L and large V_c and thus low L^* , so that the signal is expected to decrease with decreasing K_0 . Notice that the effect of K_0 is not only through the correlation to L and V_c : the reader is referred to [44] – see in particular its section III – for an explicit analysis of all the effects.

A conservative estimate – based on the full range of B/C allowed propagation parameters – leads to variations of about two orders of magnitude of the primary antiproton flux. Notice that this does not include the nuclear and particle physics uncertainties. This range could be narrowed by using constraints coming from other species of cosmic rays. Actually, using radioactive [50] or heavy [51] species only yield a minor improvement. They enable to shrink the parameter space but leave unchanged the values leading to the extremal fluxes. The final extreme and median parameters which we have considered in this analysis are borrowed from [44]. They are displayed in Tab. II.

case	δ	K_0 [kpc ² /Myr]	L [kpc]	V_c [km/sec]
max	0.46	0.0765	15	5
med	0.70	0.0112	4	12
min	0.85	0.0016	1	13.5

TABLE II: Astrophysical parameters giving the maximal, median and minimal LKP antiproton flux compatible with B/C analysis.

IV. FLUX AND CONCLUSIONS

The case of UED models is featured in Fig. 1 to 3 where the LKP mass has been set equal to 300 GeV and to 1 TeV. The interstellar antiproton yields are plotted as a function of interstellar kinetic energy $T_{\bar{p}}^{\text{IS}}$ for three different halo profiles. The canonical isothermal, NFW and Moore models respectively correspond to the solid blue, dashed red and dot-dashed magenta curves. The solid black line is the conventional secondary component. We have somewhat improved the previous estimate [21] by taking adiabatic losses into account. The maximum, median and minimum diffusion configurations respectively correspond to Fig. 1, 2 and 3. A few remarks are in order.

To commence, because the square of the LKP mass enters into the denominator of the $B^{(1)}$ annihilation cross section – see relation (2) – the antiproton source term $q_{\bar{p}}^{\text{LKP}}$ varies globally like M_{LKP}^{-4} . As a consequence, when the LKP mass is increased from 300 GeV to 1 TeV, the antiproton fluxes drop by a factor of $(10/3)^4 \sim 120$. This downward shift of the curves by two orders of magnitude is clearly present in the figures.

Then, as already discussed in section III, the particular choice for the galactic cosmic ray diffusion parameters strongly affects the primary yields whereas the secondary component varies very little. From the maximal to the minimal configurations – see Tab. II – primary antiproton fluxes decrease by two orders of magnitude. That sensitivity combined with fairly similar shapes for the primary and secondary energy spectra do not strengthen the case of the antiproton signal as a clear signature for UED dark matter. Even in the most favorable case of a 300 GeV $B^{(1)}$ boson and for maximal galactic diffusion – see Fig. 1 – the secondary background overcomes the primary LKP signal up to an antiproton kinetic energy of 100 GeV. Notice however that above that energy and in the case of a Moore halo profile, the signal may eventually become comparable to the background, leading to an excess of antiprotons at high energy that has already been noticed by [52]. Unfortunately, that distinctive spectral feature vanishes as soon as other configurations for the galactic cosmic ray propagation are selected. In Fig. 3, the antiproton yield is ~ 30 times smaller than the secondary flux for an antiproton kinetic energy of 100 GeV.

Finally, the cusp at the Milky Way center does not affect much the primary antiproton signal. Varying the DM halo profile from a mild canonical isothermal distribution to the extreme case of a Moore divergence results in an increase of the primary yields by at most a factor ~ 2 to 3 in the case of maximal galactic diffusion. That increase is much less significant for the median diffusion case and has disappeared in Fig. 3. As is clear in Tab. II, the minimal diffusion configuration corresponds to a thickness of the confinement layers of only 1 kpc associated with a strong galactic convection wind that wipes away any particle originating from the galactic central cusp.

Notice that our galactic diffusion code relies on the expansion of the radial dependence of the cosmic ray abundances as a series of the Bessel functions $J_0(\alpha_i r/R_{\text{gal}})$ where α_i is the i -th zero of the function J_0 and where R_{gal} is the radius of the propagation region. Because taking properly into account a central divergence like $r^{-2\gamma}$ with $\gamma = 1$ – NFW – or 1.3 – Moore – would necessitate an infinite number of such functions in the above expansion and would lead to numerical instability, we have renormalized the DM distribution in the vicinity of the Milky Way center without modifying the absolute number of its annihilations. More precisely, the actual DM density within a sphere of radius r_c is given by

$$\frac{\rho(r)}{\rho_c} = \left\{ \frac{r_c}{r} \right\}^\gamma, \quad (4)$$

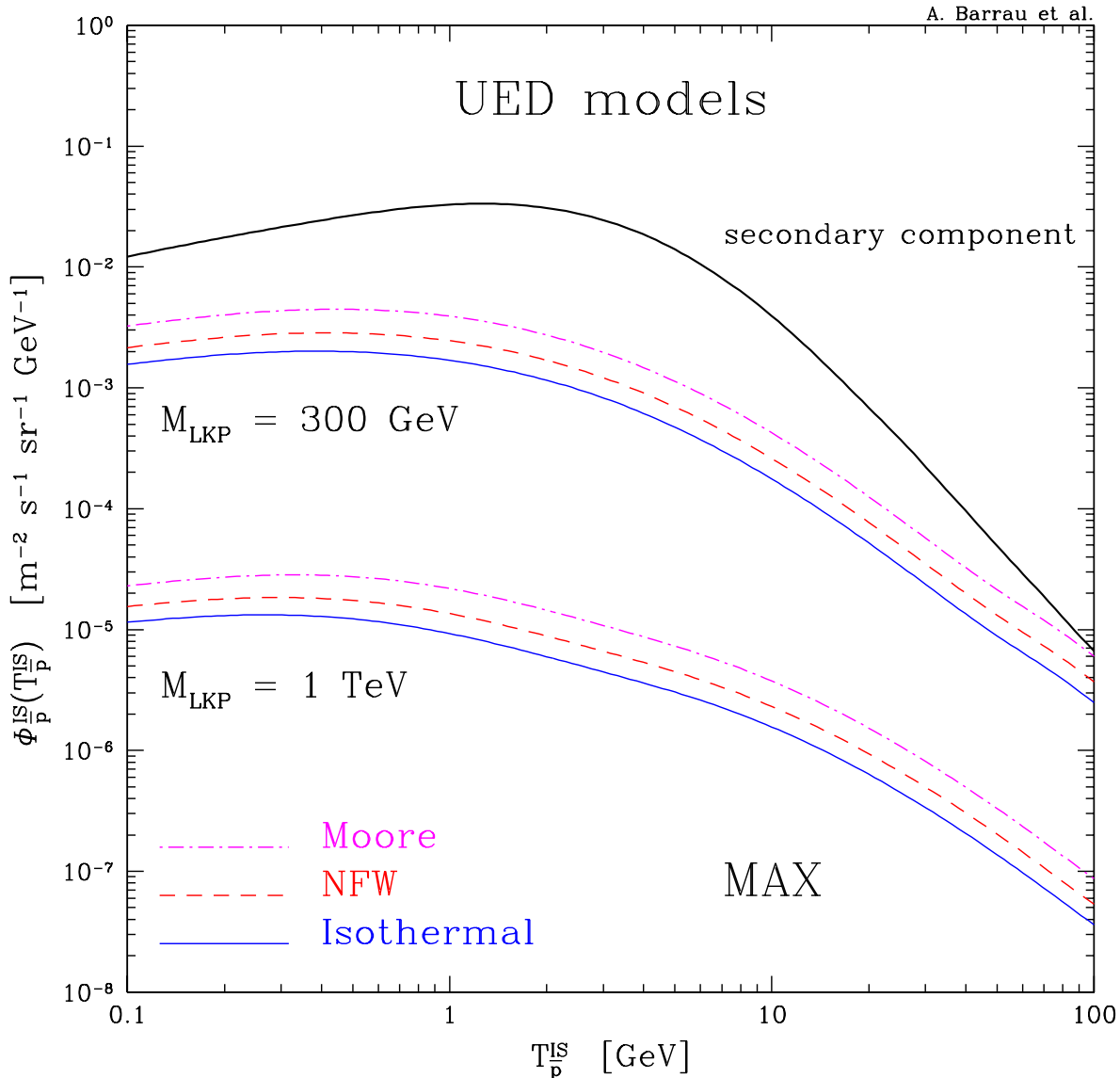


FIG. 1: The primary interstellar antiproton flux is featured as a function of the antiproton kinetic energy T_p^{IS} for a LKP mass of 300 GeV and 1 TeV. Maximal values for the diffusion parameters have been assumed here – see Tab. II. The three different halo profiles that have been selected in this calculation are described in Tab. I. The IS secondary component is the solid black line that overcomes the primary fluxes.

where $\rho_c \equiv \rho(r_c)$. The central cusp boosts the LKP annihilations by a factor of

$$\eta = \frac{3}{3 - 2\gamma} \quad (5)$$

with respect to the case of a uniform distribution with constant density ρ_c . We have replaced the divergent distribution (4) by the milder profile

$$\left\{ \frac{\rho(r \leq r_c)}{\rho_c} \right\}^2 = 1 + \left\{ \frac{2\pi^2}{3} (\eta - 1) \text{sin}_c^2 \left(\frac{\pi r}{r_c} \right) \right\}, \quad (6)$$

where $\text{sin}_c(x) \equiv \sin(x)/x$. That renormalized density leads to the same number of LKP annihilations as the actual cusp. We have set $r_c = 500 \text{ pc}$ and our primary flux calculations converge with only $N_{\text{Bes}} = 300$ terms in the Bessel

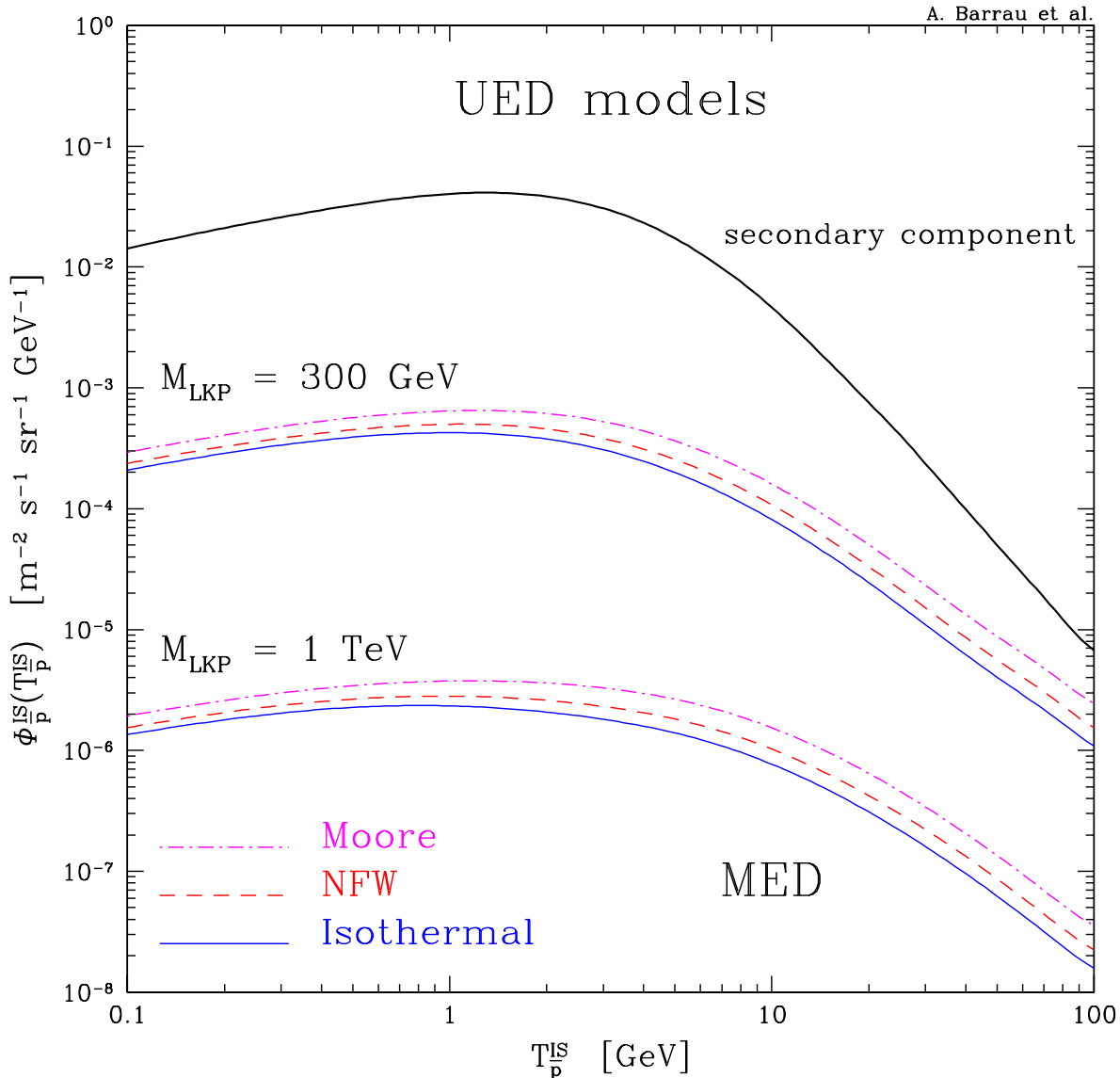


FIG. 2: The same as before but with median diffusion parameters. Primary fluxes drop by one order of magnitude.

expansion. A smaller value of r_c would require a larger N_{Bes} and is not actually necessary insofar as the antiproton Green function that connects the solar system to the galactic central region varies smoothly over the latter [45, 48]. In the minimal case for cosmic ray propagation – presented in Fig. 3 – it even vanishes.

Because of the uncertainties in the cosmic ray galactic propagation, we conclude that the antiproton signal is not the best tool to observe UED Kaluza-Klein species in the halo of the Milky Way. Direct detection is not very promising either since observable rates at current instruments are typically less than one event per year [9]. On the contrary, since a pair of $B^{(1)}$ bosons may annihilate directly into light fermions, the positron signal should exhibit a characteristic spectral spike spreading toward low energies as a result of positron energy losses during propagation [10]. Notice however that the positron annihilation signal arising in the case of an isothermal halo needs to be amplified by a factor of ~ 60 [53] before being detectable by AMS-02 [29]. An enhancement by a factor of ~ 200 with respect to a pure NFW cusp is also necessary to reproduce – albeit below 0.8 TeV [12] – the flat gamma ray spectrum which the HESS collaboration has detected at the center of the Milky Way [54]. The positron and gamma ray spectra are harder for Kaluza-Klein species than for neutralinos. Those signals have therefore been advocated as promising signatures. A word of caution is in order at that stage. The positron signature requires to be significantly enhanced in order to be detectable. If we now assume a boost factor of \sim a hundred as suggested by recent numerical simulations [55]

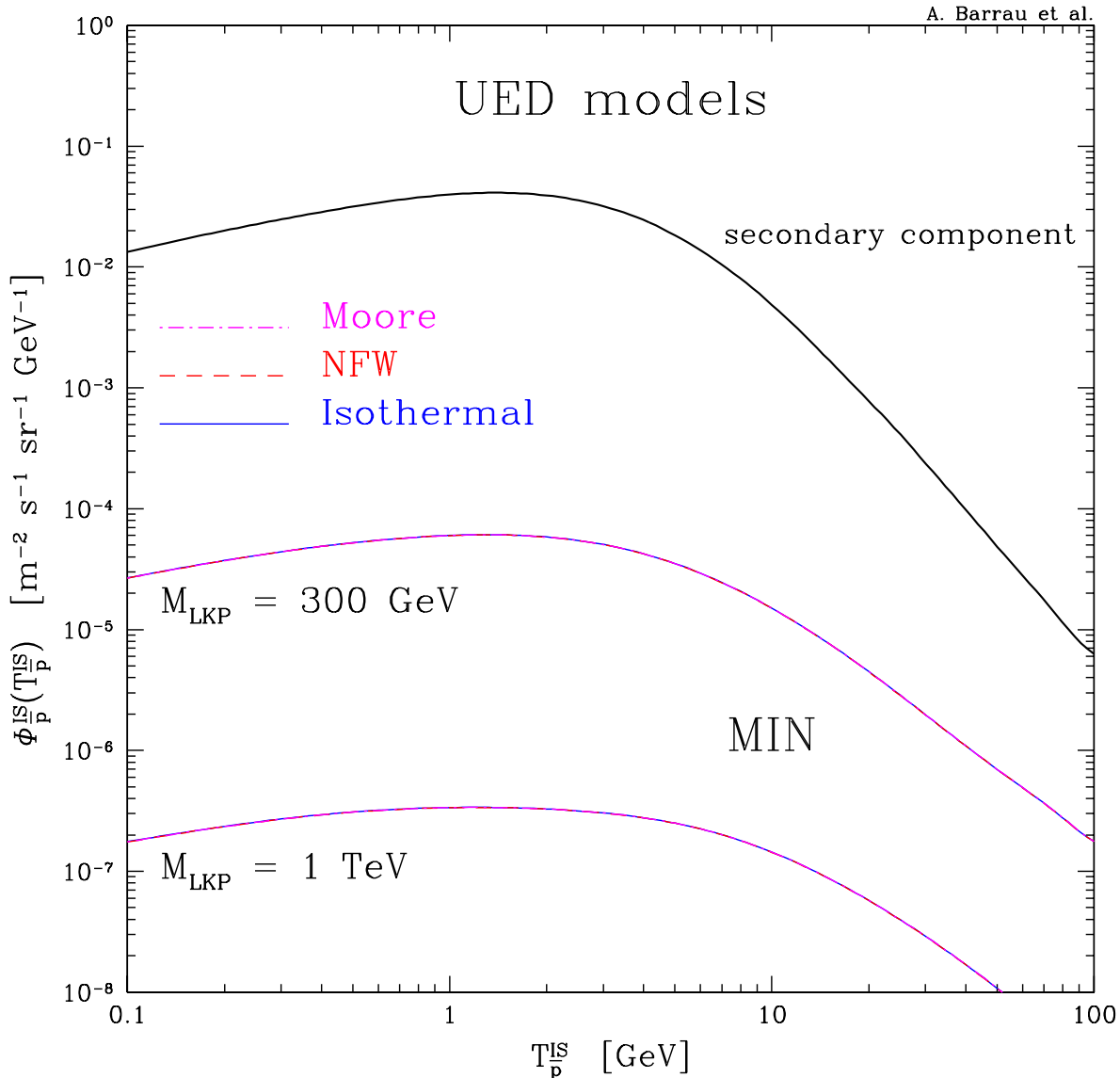


FIG. 3: The same as before but with minimum diffusion parameters. Fluxes have decreased by two orders of magnitude with respect to the maximal case. Cosmic rays no longer come from the galactic center. As a consequence, the primary component is insensitive to the sharpness of the central cusp and the three different halo profiles that have been chosen in this calculation – isothermal, NFW and Moore – lead to the same spectra.

that point toward the presence of numerous mini-clumps in the DM galactic halo, primary antiprotons should be copiously produced since even in the most pessimistic diffusion scheme of Fig. 3, the signal exceeds the background above $T_p^{IS} \sim 40$ GeV in the case of a 300 GeV $B^{(1)}$ boson.

For the warped models of [18, 19], the LZP may be much lighter than the UED dark matter candidate. The primary antiproton flux – at the top of the atmosphere – is plotted in Fig. 4 as a function of antiproton kinetic energy T_p^{TOA} for five different values of the LZP mass. The most optimistic galactic diffusion scheme as well as a canonical isothermal DM halo have been assumed for the primary signal. Observations from various experiments performed during solar minimum [24, 26, 27, 30] are well explained by the narrow band within which the background of secondary antiprotons lies irrespective of the galactic propagation conditions. The curves corresponding to $M_{LZP} = 40$ – short dashed magenta – and 50 GeV – long dashed red – exceed the background and should have already led to a detection would our assumptions on galactic diffusion and halo profile be correct. For $M_{LZP} = M_{Z^0}/2$, the LZP annihilation is actually driven by the Z -resonance and is significantly enhanced.

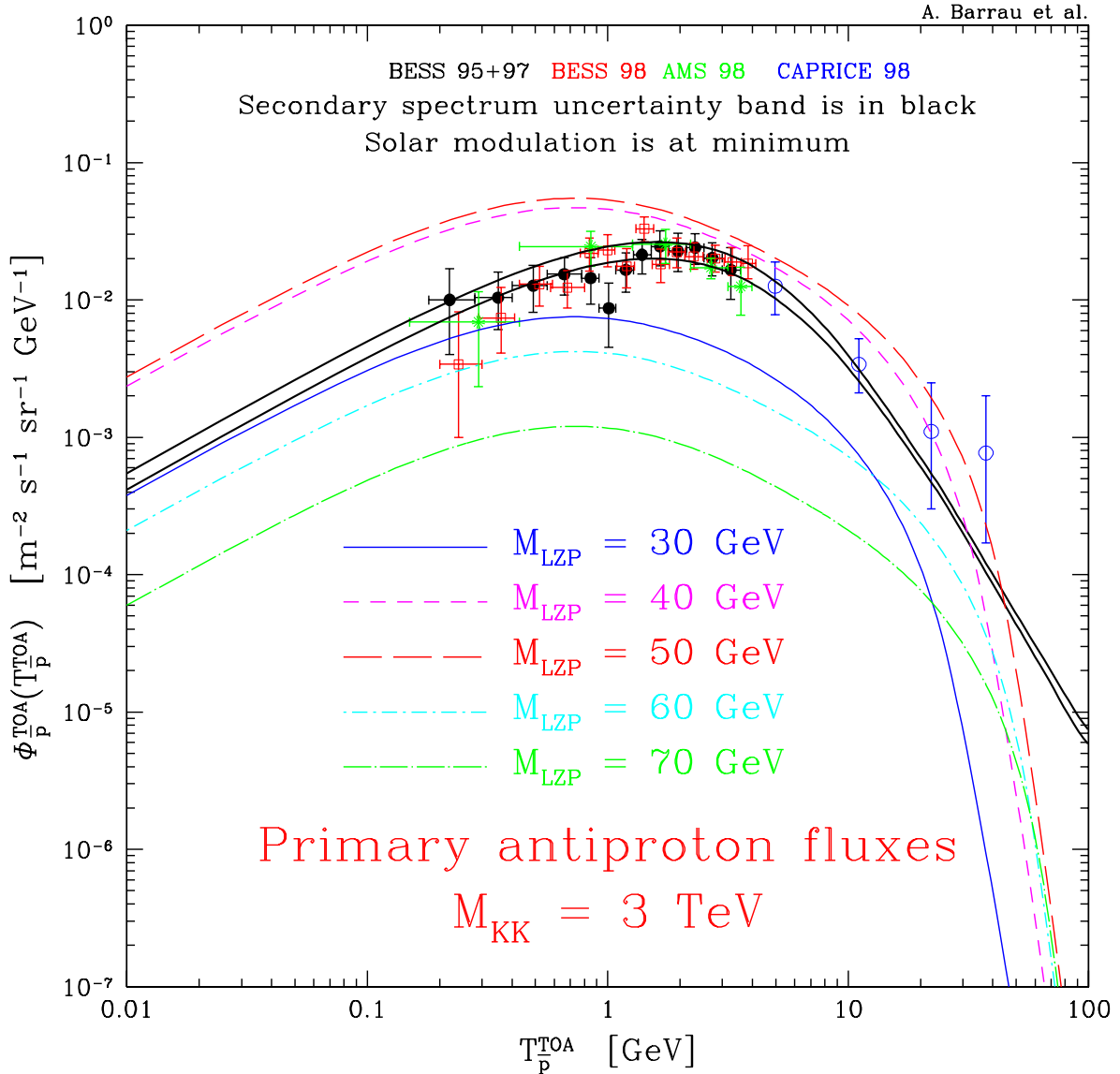


FIG. 4: The primary antiproton fluxes correspond to the warped geometry of [18, 19]. The LZP mass has been varied from 30 to 70 GeV with a Kaluza-Klein scale M_{KK} of 3 TeV. When the LZP mass is close to $M_{Z^0}/2$, the annihilation becomes resonant and the primary signal exceeds the conventional background of secondary antiprotons that lies in the narrow band within the two solid black lines. Maximal diffusion parameters have been assumed for the LZP antiproton spectra with a canonical isothermal DM distribution.

As in the previous discussion of the UED models, the LZP antiproton signal sensitively depends on galactic cosmic ray propagation. In Fig. 5, the primary yields of a 40 and 50 GeV LZP decrease by two orders of magnitude between the most optimistic and the most pessimistic diffusion cases of Tab. II. In the latter configuration, the antiproton signal is now well below the background. The halo profile is also a source of uncertainty as is clear in Fig. 6 where a 60 GeV LZP is exhibited. The maximal galactic diffusion that has been assumed in that case makes it possible for antiprotons from the central cusp to reach the solar circle and to lift the degeneracy among the various DM distributions. Should the minimal diffusion scheme be preferred, the three colored curves would be one and the same.

As featured in Fig. 4 to 6, the LZP antiproton signal is in the vicinity of the secondary background and therefore in the ballpark for detection. That is why we have explored the effect of a clumpy DM distribution by taking into account an overall boost factor in our estimates of the primary yields which we have compared to observations. We have actually performed a χ^2 test to assess the compatibility between our theoretical predictions for both secondary and primary

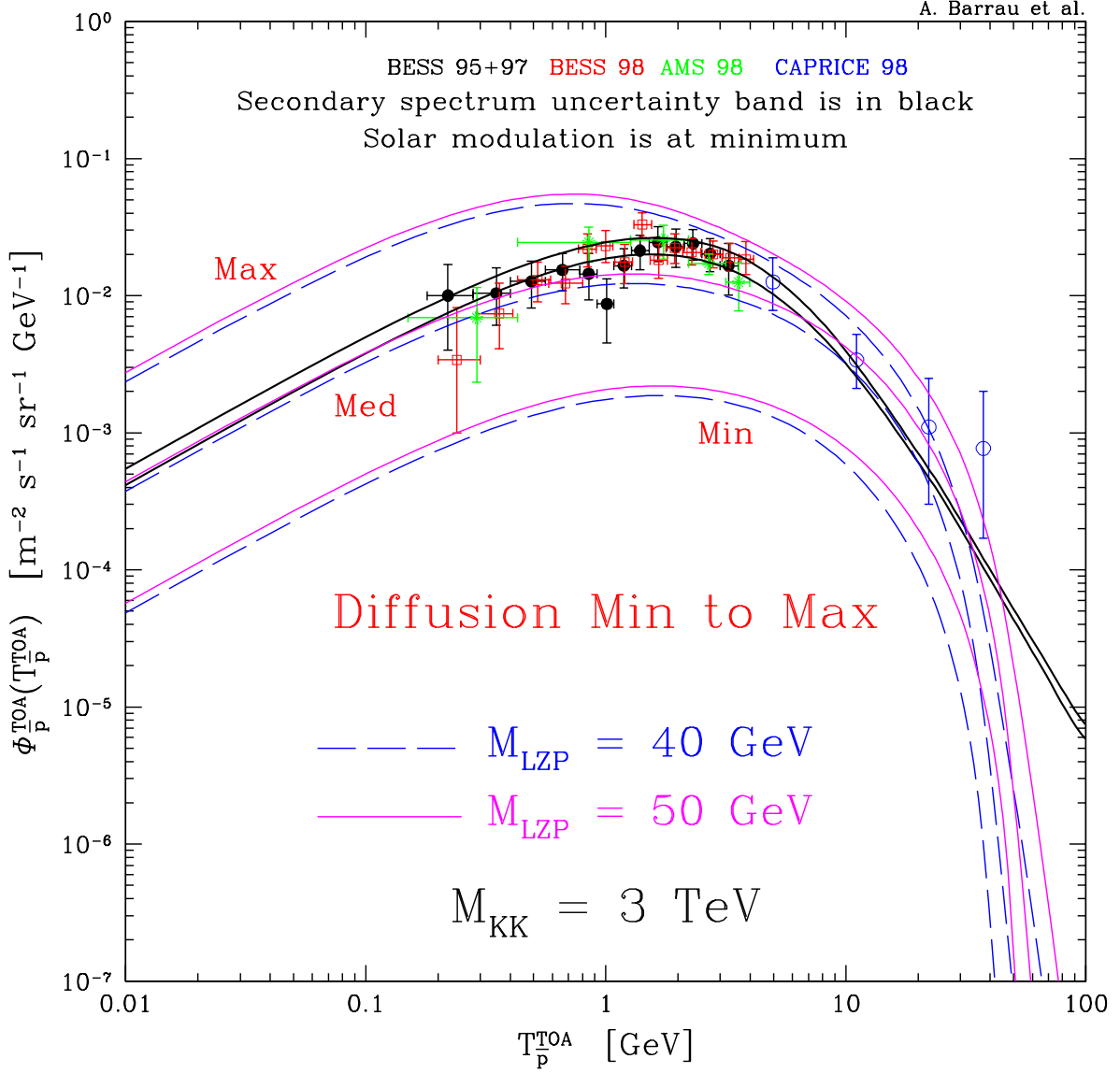


FIG. 5: When the diffusion parameters are varied over the entire domain that is compatible with the B/C ratio, antiproton primary fluxes span two orders of magnitude whilst the secondary component lies within a much narrower band. The case of a resonant LZP has been featured here with $M_{LZP} = 40$ – blue dashed – and 50 GeV – solid magenta. A canonical isothermal DM distribution has been assumed. In the case of minimal diffusion, the LZP signal is well below the background.

components and the experimental data. All the available measurements have been used [22, 23, 24, 25, 26, 27, 28, 30] except the Buffington point which is known for being one order of magnitude above all the others. Those experiments are either balloon borne – IMAX, MASS, CAPRICE and BESS – or space borne as AMS. In addition to statistical effects, they suffer from uncertainties associated with instrumental misreconstructions – *e.g.* from electrons – and from the atmosphere component contamination which has to be removed – unless only antiprotons above the geomagnetic cutoff are taken into account. Within the error bars, the IS fluxes inferred from those experiments are now in reasonable agreement. A dramatic improvement is expected in the forthcoming years with AMS-02 which will be implemented on the International Space Station for 3 years starting in 2008 : both statistic and systematic errors are expected to be reduced by several orders of magnitude for antiprotons above 0.5 GeV. To take into account the differences in solar activity between those observations, the modulation has been applied in the force field scheme with three different field values ϕ : 500 MV, 700 MV and 1000 MV, depending on the periods. The errors used are the experimental statistical uncertainties. Fig. 7 features the χ^2 per degree of freedom as a function of the boost

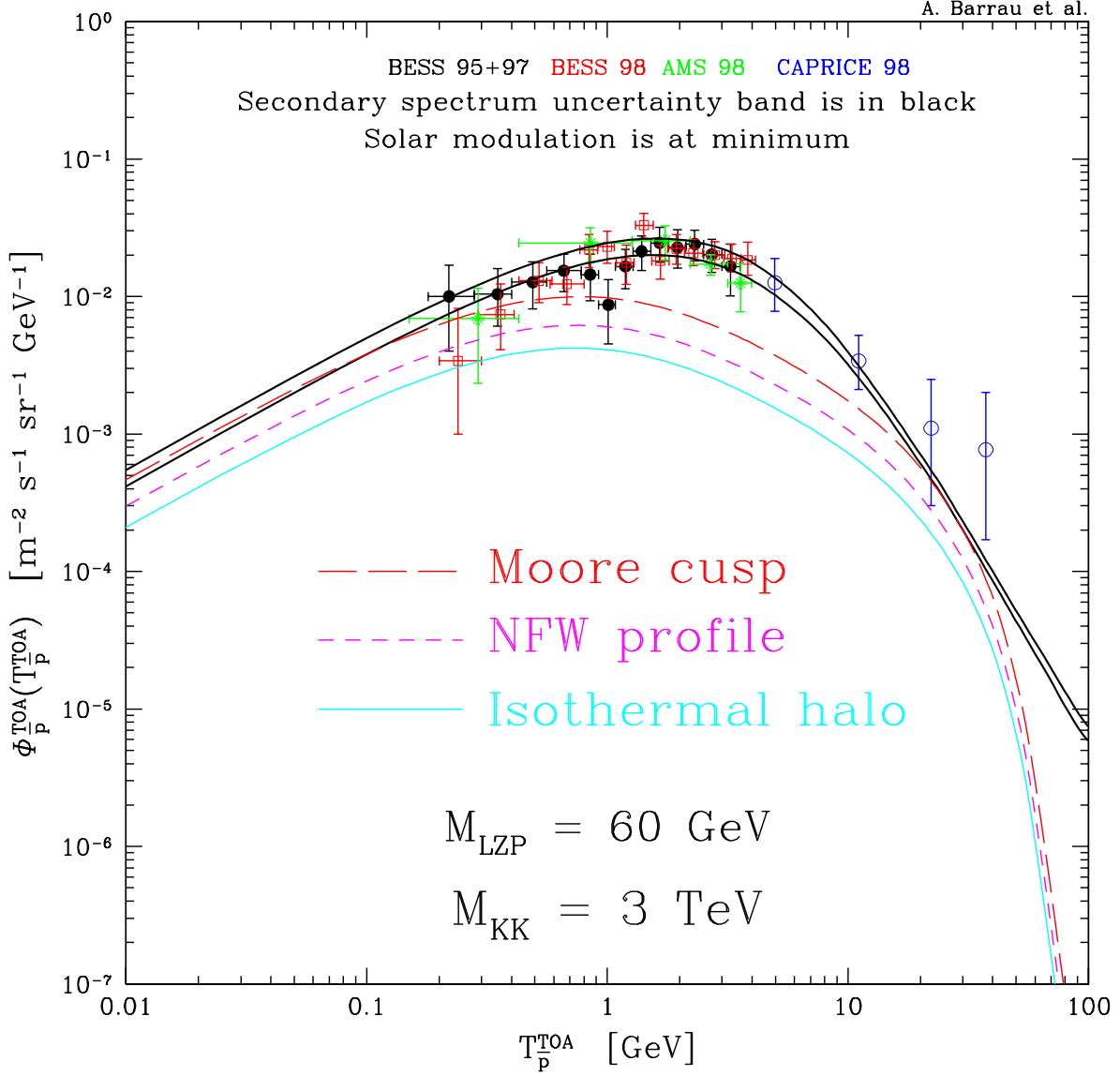


FIG. 6: The effect of the DM halo profile is presented in this figure where the mass of the LZP has been set equal to $M_{LZP} = 60$ GeV with a Kaluza-Klein scale M_{KK} of 3 TeV. The more divergent and concentrated the LZP distribution at the center of the Milky Way, the larger the antiproton yield. That effect is particularly acute in this plot where maximum diffusion parameters have been assumed.

factor for $M_{LZP} = 30$ GeV and a Kaluza-Klein scale M_{KK} of 3 TeV. The red, green and black curves respectively correspond to the maximum, median and minimum cosmic ray diffusion configurations. It should be emphasized that the value of that χ^2 must be taken with care as it indicates that the uncertainties have been underestimated, making any quantitative statistical conclusion impossible to reach. To give a crude estimate of the rejection power of this study, we have decided that models leading to a $\chi^2/\text{d.o.f.}$ larger than twice its minimum value – for the considered parameters – are excluded. In the case of a real χ^2 distribution, it would correspond roughly to the 99.9 % confidence level – we use ~ 50 degrees of freedom. In Tab. III, the LZP mass has been varied from 30 to 80 GeV whereas the Kaluza-Klein scale M_{KK} has been set equal to 3 and 6 TeV. The DM annihilation boost factor above which the primary antiproton signal is too strong to be compatible with the observations is displayed for each configuration. If a boost factor of \sim one hundred is assumed, all the configurations with $M_{KK} = 3$ TeV are excluded whereas the LZP antiproton signal is potentially detectable for larger Kaluza-Klein scales.

Notice finally that direct detection experiments already exclude almost entirely a Kaluza-Klein scale M_{KK} of 3 TeV

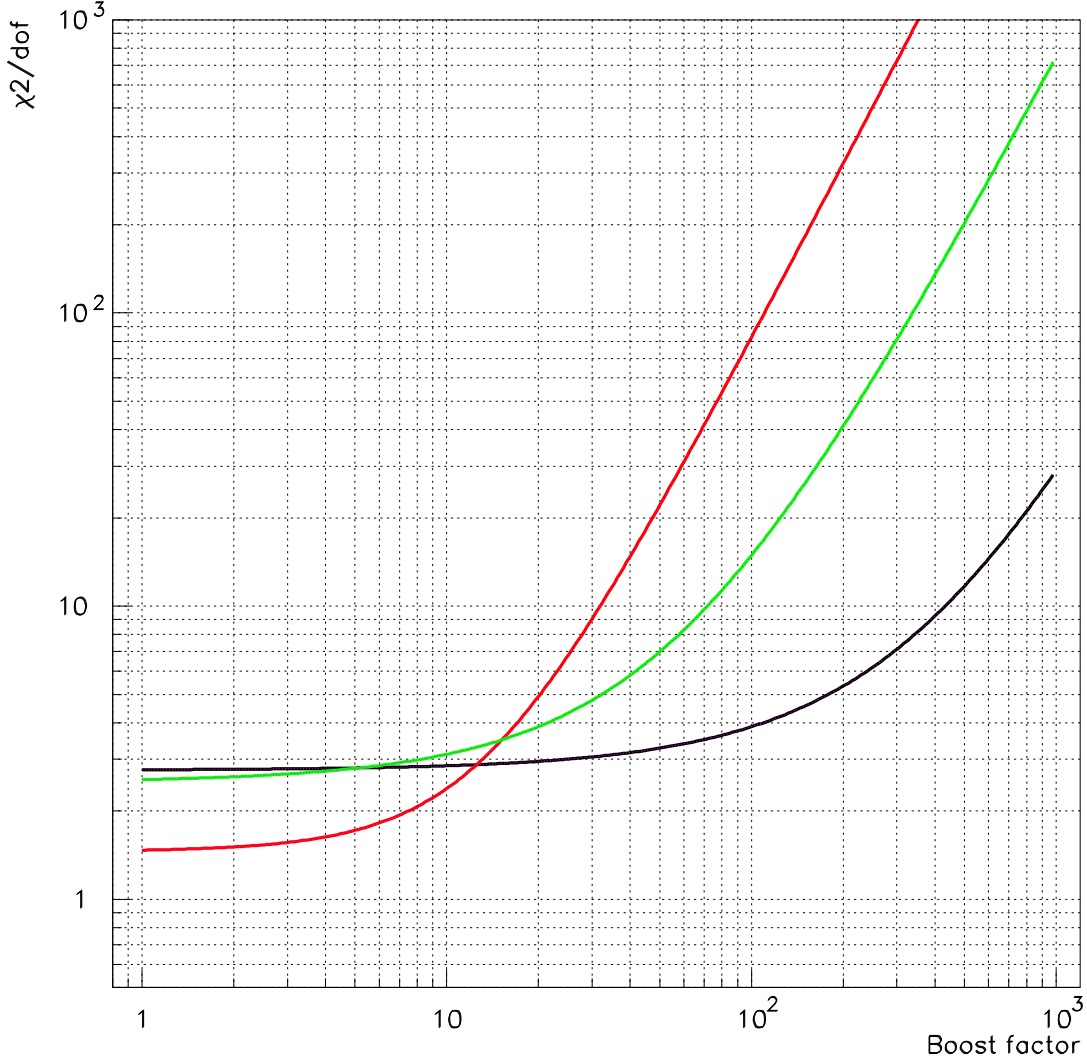


FIG. 7: The χ^2 per degree of freedom is presented as a function of the boost factor for $M_{LZP} = 30$ GeV and $M_{KK} = 3$ TeV. From top to bottom – at a boost factor of 100 – the curves correspond to the maximum, median and minimum diffusion parameters as defined in Tab. II. In the left part of the figure, the χ^2 value is dominated by the secondary component while in the right part, it is dominated by the primary component.

whereas larger values are allowed [18]. The LZP may also directly annihilate into light fermions and can produce the same kind of distortion in the positron spectrum as UED dark matter species. The HEAT excess [56, 57] is actually well reproduced by a 40 or 50 GeV LZP if the boost factor is respectively set equal to ~ 40 and 30 [20]. Antiproton calculations suffer from large uncertainties as regards the galactic cosmic ray propagation. The difficulty to reach a conclusion as regards the detectability of a primary antiproton signal has been illustrated in this article. We would like to stress that the same kind of ambiguities should also affect secondary and primary positrons with a magnitude that is yet to be determined.

LZP mass	Minimum diffusion	Median diffusion	Maximum diffusion
$M_{LZP} = 30$ GeV	$M_{KK} = 3$ TeV : 13.1 $M_{KK} = 6$ TeV : 214	$M_{KK} = 3$ TeV : 2.08 $M_{KK} = 6$ TeV : 33.10	$M_{KK} = 3$ TeV : excluded $M_{KK} = 6$ TeV : 12.9
$M_{LZP} = 40$ GeV	$M_{KK} = 3$ TeV : 2.09 $M_{KK} = 6$ TeV : 33.9	$M_{KK} = 3$ TeV : excluded $M_{KK} = 6$ TeV : 5.25	$M_{KK} = 3$ TeV : excluded $M_{KK} = 6$ TeV : 2.09
$M_{LZP} = 50$ GeV	$M_{KK} = 3$ TeV : 1.74 $M_{KK} = 6$ TeV : 27.5	$M_{KK} = 3$ TeV : excluded $M_{KK} = 6$ TeV : 4.27	$M_{KK} = 3$ TeV : excluded $M_{KK} = 6$ TeV : 2.70
$M_{LZP} = 60$ GeV	$M_{KK} = 3$ TeV : 22.9 $M_{KK} = 6$ TeV : 355	$M_{KK} = 3$ TeV : 3.55 $M_{KK} = 6$ TeV : 55.0	$M_{KK} = 3$ TeV : 1.41 $M_{KK} = 6$ TeV : 22.4
$M_{LZP} = 70$ GeV	$M_{KK} = 3$ TeV : 79.4 $M_{KK} = 6$ TeV : 1240	$M_{KK} = 3$ TeV : 12.3 $M_{KK} = 6$ TeV : 191	$M_{KK} = 3$ TeV : 5.01 $M_{KK} = 6$ TeV : 78.2
$M_{LZP} = 80$ GeV	$M_{KK} = 3$ TeV : 191 $M_{KK} = 6$ TeV : 2930	$M_{KK} = 3$ TeV : 29.3 $M_{KK} = 6$ TeV : 464	$M_{KK} = 3$ TeV : 12.0 $M_{KK} = 6$ TeV : 185

TABLE III: Boost factor above which the LZP model is excluded. The condition that $\chi^2/\text{d.o.f.} \geq 2 \times \chi_{\min}^2/\text{d.o.f.}$ is required. Different galactic diffusion schemes have been considered. An isothermal DM halo profile is assumed.

Acknowledgements : P.S. would like to thank the french programme national de cosmologie PNC and the groupement de recherche on phénomènes cosmiques de haute énergie PCHE for their financial support.

-
- [1] W. L. Freedman and M. S. Turner, *Rev. Mod. Phys.* **75**, 1433 (2003).
[2] D. N. Spergel *et al.*, *Astrophys. J. Suppl.* **148**, 175 (2003).
[3] T. Appelquist, H. C. Cheng, and B. A. Dobrescu, *Phys. Rev. D* **64**, 035002 (2001).
[4] L. Randall and R. Sundrum, *Phys. Rev. Lett.* **83**, 3370 (1999).
[5] N. Arkani-Hamed, S. Dimopoulos, and G. R. Dvali, *Phys. Lett. B* **429**, 263 (1998).
[6] H. C. Cheng, K. T. Matchev, and M. Schmaltz, *Phys. Rev. D* **66**, 036005 (2002).
[7] G. Servant and T. M. P. Tait, *Nucl. Phys. B* **650**, 391 (2002).
[8] M. Kakizaki, S. Matsumoto, Y. Sato, and M. Senami, [arXiv:hep-ph/0502059](https://arxiv.org/abs/hep-ph/0502059) (2005).
[9] G. Servant and T. M. P. Tait, *New J. Phys.* **4**, 99 (2002).
[10] H.-C. Cheng, J. L. Feng, and K. T. Matchev, *Phys. Rev. Lett.* **89**, 211301 (2002).
[11] G. Bertone, G. Servant, and G. Sigl, *Phys. Rev. D* **68**, 044008 (2003).
[12] L. Bergstrom, T. Bringmann, M. Eriksson, and M. Gustafsson, *Phys. Rev. Lett.* **94**, 131301 (2005).
[13] E. A. Baltz and D. Hooper, [arXiv:astro-ph/0411053](https://arxiv.org/abs/astro-ph/0411053) (2004).
[14] L. Bergstrom, T. Bringmann, M. Eriksson, and M. Gustafsson, *JCAP* **04**, 004 (2005).
[15] D. Hooper and G. D. Kribs, *Phys. Rev. D* **70**, 115004 (2004).
[16] D. Hooper and G. D. Kribs, *Phys. Rev. D* **67**, 055003 (2003).
[17] E. W. Kolb, G. Servant, and T. M. P. Tait, *JCAP* **07**, 008 (2003).
[18] K. Agashe and G. Servant, *Phys. Rev. Lett.* **93**, 231805 (2004).
[19] K. Agashe and G. Servant, *JCAP* **02**, 002 (2005).
[20] D. Hooper and G. Servant, [arXiv:hep-ph/0502247](https://arxiv.org/abs/hep-ph/0502247) (2005).
[21] F. Donato, D. Maurin, P. Salati, A. Barrau, G. Boudoul, and R. Taillet, *Astrophys. J.* **563**, 172 (2001).
[22] IMAX Collaboration – J. W. Mitchell *et al.*, *Phys. Rev. Lett.* **76**, 3057 (1996).
[23] MASS Collaboration – G. Basini *et al.*, *Proceedings of the 26th ICRC* (1999).
[24] CAPRICE Collaboration – M. Boezio *et al.*, *Astrophys. J.* **561**, 787 (2001).
[25] CAPRICE Collaboration – M. Boezio *et al.*, *Astrophys. J.* **487**, 415 (1997).
[26] BESS Collaboration – S. Orito *et al.*, *Phys. Rev. Lett.* **84**, 1078 (2000).
[27] BESS Collaboration – T. Maeno *et al.*, *Astropart. Phys.* **16**, 121 (2001).
[28] BESS Collaboration – Y. Asoaka *et al.*, *Phys. Rev. Lett.* **88**, 051101 (2002).
[29] AMS Collaboration, <http://pcamss0.cern.ch/mm.html> (2005).
[30] AMS Collaboration – M. Aguilar *et al.*, *Phys. Rep.* **366**, 331 (2002).
[31] T. Tjostrand, *Comput. Phys. Commun.* **82**, 74 (1994).
[32] J. F. Navarro, C. S. Frenk, and S. D. M. White, *Astrophys. J.* **462**, 563 (1996).
[33] T. Fukushige and J. Makino, *Astrophys. J.* **477**, L9 (1997).
[34] B. Moore *et al.*, *Mon. Not. Roy. Astron. Soc.* **310**, 1147 (1999).
[35] J. Diemand, B. Moore, and J. Stadel, *Mon. Not. Roy. Astron. Soc.* **353**, 624 (2004).
[36] J. F. Navarro, E. Hayashi, C. Power, A. R. Jenkins, C. S. Frenk, S. D. M. White, V. Springel, J. Stadel, and T. R. Quinn, *Mon. Not. Roy. Astron. Soc.* **349**, 1039 (2004).

- [37] A. Borriello and P. Salucci, *Mon. Not. Roy. Astron. Soc.* **323**, 285 (2001).
- [38] W. J. G. de Blok and A. Bosma, *Astron. Astroph.* **385**, 816 (2002).
- [39] R. A. Swaters *et al.*, *Astrophys. J.* **583**, 732 (2003).
- [40] D. T. F. Weldrake, W. J. G. de Blok, and F. Walter, *Mon. Not. Roy. Astron. Soc.* **340**, 12 (2003).
- [41] G. Gentile, P. Salucci, U. Klein, D. Vergani, and P. Kalberla, *Mon. Not. Roy. Astron. Soc.* **351**, 903 (2004).
- [42] F. Donato, G. Gentile, and P. Salucci, *Mon. Not. Roy. Astron. Soc.* **353**, L17 (2004).
- [43] J. N. Bahcall and R. M. Soneira, *Astrophys. J. Suppl.* **44**, 73 (1980).
- [44] F. Donato, N. Fornengo, D. Maurin, P. Salati, and R. Taillet, *Phys. Rev. D* **69**, 063501 (2004).
- [45] D. Maurin and R. Taillet, *Astron. Astroph.* **404**, 949 (2003).
- [46] D. Maurin, R. Taillet, F. Donato, P. Salati, A. Barrau, and G. Boudoul, *Research Signpost astro-ph/0212111* (2003).
- [47] D. Maurin, F. Donato, R. Taillet, and P. Salati, *Astrophys. J.* **555**, 585 (2001).
- [48] R. Taillet and D. Maurin, *Astron. Astroph.* **402**, 971 (2003).
- [49] F. C. Jones, *Astrophys. J.* **222**, 1097 (1978).
- [50] F. Donato, D. Maurin, and R. Taillet, *Astron. Astroph.* **381**, 539 (2002).
- [51] C. Combet, D. Maurin, J. Donnelly, L. O’C. Drury, and E. Vangioni-Flam, *Astron. Astroph.* **435**, 151 (2005).
- [52] T. Bringmann, [arXiv:astro-ph/0506219](https://arxiv.org/abs/astro-ph/0506219) (2005).
- [53] J. Pochon, Ph.D. thesis - Chapter 9 (2005).
- [54] HESS Collaboration – F. Aharonian *et al.*, *Astron. Astroph.* **425**, L13 (2004).
- [55] J. Diemand, B. Moore, and J. Stadel, *Nature* **433**, 389 (2005).
- [56] HEAT Collaboration – S. W. Barwick *et al.*, *Astrophys. J.* **482**, L191 (1997).
- [57] S. Coutu *et al.*, *Astropart. Phys.* **11**, 429 (1999).